The Prediction of Broadband Shock-Associated Noise from Dualstream and Rectangular Jets using RANS CFD

Steven A. E. Miller*

The National Aeronautics and Space Administration, Hampton, Virginia 23681, USA

Philip J. Morris†

The Pennsylvania State University, University Park, Pennsylvania 16802, USA

Supersonic jets operating off-design produce broadband shock-associated noise. Broadband shock-associated noise is characterized by multiple broadband peaks in the far-field and is often the dominant source of noise towards the sideline and upstream direction relative to the jet axis. It is due to large scale coherent turbulence structures in the jet shear layers interacting with the shock cell structure. A broadband shock-associated noise model recently developed by the authors predicts this noise component from solutions to the Reynolds averaged Navier-Stokes equations using a two-equation turbulence model. The broadband shock-associated noise model is applied to dualstream and rectangular nozzles operating supersonically, heated, and off-design. The dualstream jet broadband shock-associated noise predictions are conducted for cases when the core jet is supersonic and the fan jet is subsonic, the core jet is subsonic and the fan jet is supersonic, and when both jet streams operate supersonically. Rectangular jet predictions are shown for a convergent-divergent nozzle operating both over- and under-expanded for cold and heated conditions. The original model implementation has been heavily modified to make accurate predictions for the dualstream jets. It is also argued that for over-expanded jets the oblique shock wave attached to the nozzle lip contributes little to broadband shock-associated noise. All predictions are compared with experiments.

I. Introduction

Broadband shock-associated noise (BBSAN) is present in supersonic jets operating at off-design conditions. It can occur for either convergent or convergent-divergent nozzles. Under these conditions the pressure at the jet exit differs from the ambient value. This imbalance generates a system of shocks and expansions in the jet plume. The interaction between the turbulence in the jet shear layer and this shock cell structure is the source of shock-associated noise. Shock-associated noise is observed in the far-field as a broad spectral peak at relatively large angles to the jet downstream axis. The peak frequency is a function of the jet shock cell spacing and the convection velocity of the jet shear layer turbulence. The amplitude of BBSAN depends on the ratio of the jet diameter to the observer distance, the polar and azimuthal observer angle, the fully expanded jet velocity, the jet diameter, and the degree of off-design operation. The last dependence is quantified by the factor,

$$\beta = \sqrt{|M_j^2 - M_d^2|} \tag{1}$$

where, M_j is the fully-expanded jet Mach number, which depends solely on the jet pressure ratio, and M_d is the nozzle design Mach number. The first prediction scheme for BBSAN was developed by Harper-Bourne and Fisher.[1] Their proposition was that BBSAN depends on the nearly coherent interaction between the turbulence in the jet shear layer and the jets nearly periodic shock cell structure. This can be modeled as

---

*Research Aerospace Engineer, Aeroacoustics Branch, NASA Langley Research Center MS 461, AIAA Member.

†A. D. Welliver / Boeing Professor of Aerospace Engineering, Aerospace Engineering, 233 Hammond Building, AIAA Fellow.

American Institute of Aeronautics and Astronautics

a series of correlated point sources that radiate either constructively or destructively. Harper-Bourne and Fisher's prediction scheme depends on knowledge of the rate of decay of the turbulence correlation between shocks, as well as the characteristic spectral shape of the radiated noise generated by each interaction. These were obtained using a least squares procedure to match the model with experimental noise measurements. The method is used in the SAE ARP876[2] prediction for single stream shock-associated noise from convergent nozzles at supercritical conditions and was also used in the original version of the Aircraft Noise Prediction Program (ANOPP).[3]

A second prediction method for shock-associated noise was developed by Tam.[4] The basic physical model was described by Tam and Tanna.[5] Tam argued that the shock cell structure in the jet could be modeled, following the work of Pack,[6] as a waveguide, where the waves are forced by the pressure imbalance at the jet exit and are confined by the jet shear layer. The simplest model that can be used for the jet is a vortex sheet. The effects of the slow divergence of the jet and the dissipative effects of the turbulence on the shock cells can also be included in the same general framework as shown by Tam, Jackson, and Seiner.[7] The large-scale turbulence in the jet shear layer is modeled as a random superposition of instability waves supported by the jet mean flow, as described by Tam and Chen.[8] The interaction between the downstream traveling instability waves and the nearly periodic shock cell structure results in an interference pattern of traveling waves. The phase velocity of these waves can be higher than that of the instability waves alone and gives rise to noise radiation at large angles to the jet downstream axis, including the upstream direction. Since there is a random set of instability waves interacting with the shock cells, the resulting radiation pattern involves broad lobes rather than a sharply directional radiation. Tam argued that a complete calculation of the large scale turbulence spectrum would be computationally very expensive. So the eventual prediction formula is based on a simple shape to represent the spectrum and empirical formulas for the shock cell spacing and convection velocity of the turbulence. In addition, the spectral width is determined with a best fit to the measured noise data. The predictions give good agreement with noise measurements in both the jet's near and far fields and certain key features of the measured spectra are captured. These include the variation of the frequency of the broadband spectral peak with observer location (the same prediction is provided by the Harper-Bourne and Fisher[1] model), the narrowing of the width of the noise spectrum as the observer moves towards the jet upstream direction, the presence of multiple lobes in the near field noise contours, and the presence of secondary spectral peaks at higher frequencies than the main peak. It should be noted that the Harper-Bourne and Fisher[1] model predicted multiple harmonics of the shock peak with the same amplitude, which is not observed in the experiments. More recent versions of ANOPP have incorporated Tam's BBSAN model.

Tam[9] modified the model by Tam[4] to include the capability to predict BBSAN from jets with more than slight heating and operating with a moderate off-design parameter. This was accomplished by better approximating the shock cell spacing to account for higher off-design parameters. Also, a temperature correction factor, T_{cf}, was included to correct the over prediction at all frequencies due to increasing total temperature ratio (TTR). Another important modification was the use of different scaling factors that were dependent on the jet being over- or under-expanded.

Dualstream jet Reynolds Averaged Navier-Stokes (RANS) calculations have recently been performed by Abdelhamid and Ganz[10] to investigate the characteristics of the shock containing plumes. It was shown that the shock cell spacing and strength was predicted correctly over a wide range of operating conditions. Clearly, as in the axisymmetric case, RANS calculations can capture realistic meanflow values for the BBSAN prediction. In dualstream jets there are essentially two sets of BBSAN sources, one due to the outer shear layer that divides the fan plume and the ambient and another due to the inner shear layer that divides the jet and fan plumes. Tam *et al.*[11] confirmed this by predicting the peak frequencies from dualstream jets where the primary stream is subsonic and the secondary stream is supersonic and operating off-design. This was performed by accurately predicting the peak BBSAN frequencies for both sets of shock wave shear layer interactions over a wide range of observer angles.

Only one successful rectangular jet BBSAN prediction model has thus far been developed. Tam and Reddy[12] developed a rectangular jet BBSAN prediction model for aspect ratios, AR, less than six and with straight side walls. The model is a modification of the work performed by Tam.[4] The model is linked to the straight wall geometry of the rectangular nozzle which always supports a shock cell structure. It consists of one shock cell structure originating from the nozzle lip when operating off-design. The second shock cell structure originates from the nozzle throat and exists even if the jet is operating on-design. Further modifications to this model have been made to include the effects of forward flight.

American Institute of Aeronautics and Astronautics

None of these models contain a method that directly connects the noise predictions to the details of the flow-field or nozzle geometry. Though, the dualstream frequency prediction method of Tam *et al.*[11] connects the Fourier transform of the shock pressure, p_s, with the BBSAN frequency. It also should be noted that Tam and Pastouchenko[11] showed that Tam and Tanna's model[5] could be applied to dual-stream jets. Recently a new method to predict BBSAN was developed by Morris and Miller[13] that used RANS-CFD to describe the properties of the jet flowfield including the shock cell structure. This method was only applied to axisymmetric jets but was developed for any type of flowfield. In theory, any complicated nozzle geometry that can produce a RANS solution can yield a BBSAN prediction. The model was evaluated extensively over a large range of single stream jet operating conditions. Most importantly, it connects the details of the flow-field, nozzle geometry, and operating conditions to the far-field spectral density.

In the present paper the model developed by Morris and Miller[13] is used to make predictions of BBSAN from supersonic dualstream and rectangular jets operating off-design. This method makes predictions based on flowfield information provided by a steady RANS Computational Fluid Dynamics (CFD) calculation. The method draws heavily on the insight into the noise generation mechanisms that are the basis of the Harper-Bourne and Fisher[1] and Tam[4] models. A short review of the model equation and the modification of its implementation for rectangular and dualstream jets are described. Results for a dualstream nozzle and a rectangular nozzle with various operating conditions are then presented.

II.   Methodology and Implementation

Here, a brief overview of the development of the BBSAN model is given. The full details are presented in Morris and Miller[13] or Miller.[14] The BBSAN model builds on the analysis of Tam[4] and is considerably simplified by using the inviscid compressible equations of motion,

$$\frac{D\pi}{Dt} + \frac{\partial v_i}{\partial x_i} = 0 \tag{2}$$

$$\frac{Dv_i}{Dt} + a^2 \frac{\partial \pi}{\partial x_i} = 0 \tag{3}$$

where D/Dt is the material derivative, t is the time, a is the local speed of sound, v_i are the velocity components in the x_i directions, $\pi = (1/\gamma)ln(p/p_\infty)$, γ is the ratio of specific heats, p is the static pressure, and p_∞ is the ambient static pressure. The instantaneous flow-field is decomposed into four parts that consist of the mean denoted by an overbar, the perturbation value associated with the shocks denoted by a subscript s, the fluctuating value associated with the turbulence denoted by a subscript t, and a final fluctuating value associated with the interaction of the shocks and the turbulence. The last term is the broadband shock-associated noise and is denoted by a prime. The mean and fluctuating quantities are substituted into Eqs. 2 and 3 and rearranged so that the left hand side is the Linearized Euler equations and the right hand side is the source terms. The source of BBSAN is a term in the momentum equation on the right hand side of the resulting equation and is,

$$f_i^v = -v_{sj}\frac{\partial v_{ti}}{\partial x_j} - v_{tj}\frac{\partial v_{si}}{\partial x_j} \tag{4}$$

The solution to the inhomogeneous form of the LEE can be written in terms of the periodic vector Green's function, $\pi_g^n(\underline{x}, \underline{y}, \omega)$, in terms of the fluctuation pressure in the far-field. The autocorrelation of the far-field pressure is formed and depends on the two point cross-correlation of f_n^v. This quantity is dependent on the strength of the shock cells and the turbulent velocity fluctuations whose product is significant in regions where the shocks and expansions intersect in the turbulent shear layer. The inverse Fourier transform of the autocorrelation of the far-field acoustic pressure is,

$$S(\underline{x}, \omega) = \frac{\rho_\infty^2 a_\infty^4}{2\pi} \int_{-\infty}^{\infty} ... \int_{-\infty}^{\infty} \sum_{n=1}^{3} \sum_{m=1}^{3} \pi_g^n(\underline{x}, \underline{y}, \omega_1) \pi_g^m(\underline{x}, \underline{z}, \omega_2)$$
$$\times \overline{f_n^v(\underline{y}, \tau_1) f_m^v(\underline{z}, \tau_2)} \delta(\omega - \omega_2) \exp[-i(\omega_1 + \omega_2)t]$$
$$\times \exp[i\omega_1\tau_1 + i\omega_2\tau_2] d\omega_1 d\omega_2 d\tau_1 d\tau_2 d\underline{y}d\underline{z} \tag{5}$$

American Institute of Aeronautics and Astronautics

The Green's functions could be calculated numerically for a given mean flow. This could involve a locally parallel approximation or the full diverging flow. Also, the problem could be formulated in terms of the adjoint Green's function for the linearized Euler equations as described by Tam and Auriault.[15] However, BBSAN is radiated predominantly at large angles to the jet downstream axis where the refractive effects of the mean flow would be small or absent, at least for single stream jets. In view of this, the vector Green's function is approximated by the Green's function in the absence of a mean flow. The components of the vector Green's function are then readily related to the Green's function of the Helmholtz equation. Also, from the form of f_i^v given by Eqn. 4, and on dimensional grounds, it is taken to scale as,

$$f_i^v \sim \frac{p_s v_t}{p_\infty a_\infty l} \tag{6}$$

The Proudmann form for the cross-correlation is used and represents an isotropic assumption of the turbulent velocity statistics. The two point cross-correlation of f_i^v is taken to be a function of the two point cross-correlation of the turbulent velocity fluctuation. It is assumed to take the form,

$$
\begin{aligned}
R^v(\underline{y}, \underline{\eta}, \tau) &= \overline{v_x\left(\underline{y}, t\right) v_x\left(\underline{y} + \underline{\eta}, t + \tau\right)} \\
&= K \exp\left[-\left|\tau\right|/\tau_s\right] \exp\left[-\left(\xi - \bar{u}_c \tau\right)^2/l^2\right] \exp\left[-\left(\eta^2 + \zeta^2\right)^2/l_\perp^2\right]
\end{aligned}
\tag{7}
$$

where R^v is the two-point cross-correlation of the turbulent velocity fluctuations, $\underline{\eta} = \underline{\eta}(\xi, \eta, \zeta)$, K is the turbulent kinetic energy, τ is the time scale, τ_s is the time scale coefficient, l is the length scale of the streamwise coherent turbulent structures, and u_c is the convection velocity of the turbulence. Performing some integrations and simplifications yields the BBSAN model developed by Morris and Miller[13] for prediction of the spectral density $S(\underline{x}, \omega)$ of BBSAN using information from a RANS solution. It can be written,

$$
\begin{aligned}
S\left(\underline{x}, \omega\right) = \frac{1}{16\pi\sqrt{\pi}a_\infty^4 x^2} \int\limits_{-\infty}^{\infty} \cdots \int\limits_{-\infty}^{\infty} & \left\{ \frac{Kl_\perp^2}{l\tau_s} p_s\left(\underline{y}\right) \tilde{p}_s\left(k_1, y_2, y_3\right) \exp\left(ik_1 y_1\right) \right. \\
& \left. \times \frac{\omega^2 \tau_s^2 \exp\left[-l^2\left(k_1 - \omega\cos\theta/a_\infty\right)^2/4 - \omega^2 l_\perp^2 \sin^2\theta/4a_\infty^2\right]}{\left[1 + \left(1 - M_c\cos\theta + \bar{u}_c k_1/\omega\right)^2 \omega^2 \tau_s^2\right]} \right\} dk_1 d\underline{y}
\end{aligned}
\tag{8}
$$

where a_∞ is the ambient speed of sound, k_1 is the wavenumber of the shock pressure in the axial direction, p_s is the shock pressure, $\tilde{p}_s$ is the Fourier transform of the shock cell pressure in the axial direction, θ is the observer angle from the downstream jet axis, and ω is the radial frequency. l and $l_\perp$ are local characteristic length scales of the turbulence of the RANS solution. Equation 8 provides the prediction formula for the BBSAN. All of the parameters can be determined from a RANS-CFD solution. The turbulence length and times scales are related to the RANS solution through a simple dimensional model.

In the evaluation of Eq. 8 there are either three or four integrations to be performed over x, r or y, z, and k_1. Certain values of wavenumber, k_1, have very small amplitudes in the Fourier transform of p_s that do not contribute to the spectral density. When the Fourier transform of p_s is not in the range of wavenumbers of interest to BBSAN or has a small amplitude then that range is not included in the integration. Performing a full wavenumber integration is more expensive computationally and no differences in the final BBSAN solutions are apparent. After the evaluation of Eq. 8 is complete it is multiplied by a prefactor that controls the amplitude of the spectral densities, P_f. This prefactor is constant and remains the same regardless of the jet conditions or nozzle geometry. After the prefactor multiplication to the spectral density, an adjustment to the spectral density is used if the jet is heated. This is necessary because it is not clearly understood by the aeroacoustic community why BBSAN discontinues to scale with increasing TTR.. The same temperature correction factor used by Tam[9] is made for heated jets in this work.

The integration of the prediction equation is performed on structured grids that are derived from the CFD solution with constant spacing between grid points. This is done for two reasons. First, this method allows grid independence studies using the highly-resolved CFD solution databases. Second, it simplifies the calculation of the Fourier transform of p_s since the grid spacing is constant with respect to x, r or y, and z. Thus a standard discrete Fourier transform or fast Fourier transform library can be used. Also, this ensures that the radial locations of $\tilde{p}_s$ and the other field variables of the integration region are the same. Arrays that hold interpolated values in the integration regions are allocated based on the values in the parameter input file. These arrays include values in the integration region of K, ϵ, p, x, r or y, z, area, $\bar{u}$, $\tilde{p}_s$, and x_k.

The spatial coordinates of the integration and wavenumber regions are found based on the parameter input file integration ranges and the respective number of index values. The range of the wavenumber region in the axial direction is based on the minimum distance between points in the axial direction.

Recognizing that the shock cell structure has nearly a single representative shock cell spacing in the shear layer and that the sources of the BBSAN are localized in the shear layer, it is not necessary to find the wavenumber spectrum of p_s at every radial location. Instead, a single sampling of the spatial variation of p_s from the nozzle lip and along the shear layer is sufficient. The end of the spatial wavenumber region is a single point far downstream inside the decreasing radius shear layer. This method of finding the wavenumber spectrum and then applying it at all radial locations when evaluating Eq. 8 allows for only a single Fourier transform to be taken and only a single sampling of p_s on a line instead of a surface or volume. The time savings are immense and the accuracy of the BBSAN results improve dramatically. Care is taken when selecting where the start and end points of the line to sample p_s are located. For example, this sampling line should never cross a shock wave that is attached to the nozzle lip, as in over-expanded jets, but should be just outside the nozzle lip.

Unlike the axisymmetric version of the code, the three-dimensional BBSAN implementation evaluates the integrals over the three dimensional integration region and wavenumber region. Since there is an additional integral that needs to be evaluated in the z-axis direction, the run time of the computer code can increase greatly. To minimize the amount of time needed to make a three-dimensional BBSAN prediction, careful choices are made to minimize the range and number of grid points of the integration and wavenumber regions. Summation of the integration region is selective, and only includes contributions from regions where K is more than 10% its maximum value using cycling. Cycling is part of the modern Fortran standard that conditionally skips loops. This cycling technique saves a large amount of computational time. Also, the solution is found relatively quickly by specifying a limited range for the integrations over wavenumber. The wavenumber integration range is carefully chosen to only encompass peak values of the wavenumber spectrum.

In Eq. 8 the values of τ_s, l, and $l_\perp$ are related to the RANS solution and are representative of the turbulent scales of motion associated with BBSAN. An additional factor, P_f, is needed in the model to scale the amplitude of the spectral density. In Morris and Miller[13] coefficients were found based on a single jet calibration and all subsequent predictions used the coefficients based on $\tau = c_\tau K/\epsilon$, $l = c_l K^{3/2}/\epsilon$, and $l_\perp = c_{l_\perp} l$. Here, coefficients are based on the heated axisymmetric jet case of $M_d = 1.0$, $M_j = 1.50$, and $TTR = 2.20$. The values of these coefficients are $c_\tau = 0.85$, $c_l = 3.00$, $c_{l_\perp} = 0.30$, and $P_f = 10^{9/10}$. It is found that these coefficients work extremely well for a wide range of jets. The value of $c_{l_\perp}$ has never been optimized and is set from physical observations that the lateral length scales are 30% of the streamwise scales. However, when the jet is operating over-expanded then a shock wave is attached to the nozzle lip and does not contribute to the BBSAN. Instead, the shock wave is interacting with the boundary layer turbulence producing a different type of noise that is identified in the recent work of Zaman $et~al.$[16] Zaman $et~al.$ examined convergent-divergent nozzles operating in the over-expanded regime and a single convergent nozzle. All the nozzles had the same exit diameter. An excess noise that is identified as not being BBSAN in nature is found and only occurs when the shock resides inside the nozzle. The source of this noise is due to the shock oscillations due to the boundary layer turbulence attached to the nozzles divergent inner wall. Since the over-expanded jet flow is different from the under-expanded jet flow due to the attached shock, the coefficient of $c_\tau = 0.50$ and $P_f = 10^{14/10}$ are used for over-expanded predictions while the length scale coefficients remain the same. These coefficients are found in the same way as the under-expanded case but used an axisymmetric jet case of $M_d = 1.50$, $M_j = 1.30$, and $TTR = 2.20$. Interestingly, the values of the coefficients c_l and $c_{l_\perp}$ are exactly the same. It is stressed that the spectra is controlled mainly by c_τ and c_l and these are found for a single jet condition for either the over- or under-expanded cases at a single observer angle. There is no optimization process over the jet conditions or observer angles. Finally, if only the under-expanded coefficients are used then good BBSAN predictions can be found, though the peaks would be too narrow.

American Institute of Aeronautics and Astronautics

III. Results

To test the prediction model two nozzle geometries are selected. The first is a dualstream nozzle provided by the Boeing Company and the latter is a rectangular nozzle provided by The Pennsylvania State University. There is no near-field fluid dynamic data available for the dualstream nozzle operating conditions but there is total pressure data and schlieren images available for the rectangular nozzle. Comparisons of the RANS results with the experimental total pressure and Mach number plots in the region of BBSAN sources shows good agreement. CFD validation with comparisons with experiment of the Wind-US RANS solutions are omitted in this paper. However, validation results of the code for axisymmetric jets are found in Miller *et al.*[14]

To test the capabilities of the prediction scheme to predict BBSAN for dualstream jets, an axisymmetric dualstream nozzle of the Boeing Company is selected. The nozzle contour is shown about its centerline in Fig. 1 a). Both the primary and secondary nozzle contours are convergent and have design Mach numbers of unity. The streamwise and radial coordinates in Fig. 1 are normalized by the core nozzle exit diameter, D_p. The primary nozzle exit diameter is $D_p = 0.06223$ m and the secondary nozzle exit diameter is $D_s = 0.0759$ m.

For rectangular jet calculations, a converging-diverging $M_d = 1.50$ nozzle is chosen and tested at The Pennsylvania State University. The aspect ratio, AR, of the rectangular nozzle is 1.75. Figure 1 part b) illustrates that the minor axis plane is an ideally expanded converging diverging nozzle geometry while the major axis plane shows only a converging section. If the nozzle is run on-design then there will be a weak shock cell system in the core of the jet. The nozzle contour of both the major and minor axis are shown in Fig. 1 b) and c). The two cross-stream coordinates are normalized with respect to the effective diameter D_e and are based on the equivalent nozzle exit area of an axisymmetric nozzle. For this rectangular nozzle $D_e = 0.01778$ m and the minor and major axis width and height are 0.0119 m and 0.0208 m respectively.

The present numerical approach uses the Reynolds Averaged Navier-Stokes (RANS) equations and are integrated until a steady solution is achieved with the NPARC Alliance Wind-US 2.0 solver. Wind-US was developed by the NPARC Alliance which is a partnership between NASA Glenn Research Center and the U. S. Air Force Arnold Engineering Development Center, and additional contributors. A large number of validation cases of a broad range of flow-regimes have been made with the Wind-US solver by the NPARC Alliance. The Menter[17] Shear Stress Transport (SST) turbulence model is used in the present simulations. The traditional ideal gas model is used for heated air simulations with a constant γ. The turbulent Prandtl number is set in all simulations at 0.90.

Two computational grids are used for this study. The first is developed for the dualstream nozzle and the second is for the rectangular nozzle. Both computational domains extend 75 normalized diameters from the nozzle centerline in the downstream direction, 50 normalized diameters from the nozzle exit in the cross-stream direction, and 5 normalized diameters upstream from the nozzle inlet. Initial iterations are performed using a constant CFL number of 0.50. Explicit Euler time stepping using a constant time step is then used until the L^2 residual remains constant and a visual inspection of the solution appears steady. The L^2 residual is a global measure of the residual error of the governing equations of the flow-field. Grid independence studies are performed by using every other grid point in the computational domain in both the streamwise and radial directions. No difference in the steady solution between the sequenced and unsequenced grid is apparent in any of the solutions.

Boundary conditions for the simulations consist of a downstream outflow in the streamwise direction allowing the flow to exit the computational domain. This assumes that the outflow is subsonic and the free-field pressure is set as the ambient pressure. Free-stream boundary conditions are specified in the free-field where a small uniform flow at $M_\infty = 0.001$ is assumed for stability and the total ambient pressure is equal to the downstream static pressure. A standard axisymmetric boundary condition, which is essentially an inviscid wall, lies on the centerline at $y/D = 0$ for the dualstream jet case. Symmetric boundary conditions are used for the rectangular calculations to take advantage of the planes of symmetry of the minor and major axis. Heat transfer is not considered in the study and adiabatic no-slip wall boundary conditions are used on the nozzle surface. Finally, the upstream boundary condition for the nozzle inlet specifies the total pressure and total temperature of the jet with an initial inlet $M = 0.15$ normal to the inlet plane. The inlet M may fluctuate and the total values of P and T are held constant. The numerical implementation and mathematical development are shown in Nelson.[18] These boundary conditions are sufficient for a steady solution to be found when using an ideal gas.

American Institute of Aeronautics and Astronautics

Dualstream Nozzle BBSAN Calculations

The operating conditions of the dualstream nozzle are chosen so that BBSAN predictions can be made for a jet with a supersonic core and subsonic fan, subsonic core and supersonic fan, and a supersonic core and supersonic fan. The various NPR, TTR, and associated M_j of each of the dualstream cases are illustrated in Table 1. Note that a subscript p and s represents the core (primary) and fan (secondary) jet operating conditions respectively. The case names are representative of the labeling system of the authors and are ordered as they appear in the proceeding discussion and figures. Since M_d of both the core and fan nozzle is 1.00, all the supersonic jets are operating off-design and under-expanded. The model has also been extensively tested for $M_d > 1.00$. $TTR_s = 1.00$ for all the dualstream cases but can be slightly elevated in realistic aircraft engines. However, this causes no problems with calculations with various TTR_s as has been demonstrated by past single stream predictions over wide ranges of TTR and core nozzle TTR_p variations.

For each dualstream RANS calculation and BBSAN prediction listed in Table 1, associated parameters are found that are necessary to make a BBSAN prediction. These values are listed in Table 3. The first column of the table lists the case number and the second column lists the integration region number. Some dualstream cases required multiple integration regions to encompass all the BBSAN sources. This is necessary so that the integration regions do not cross over solid wall boundaries of the nozzle. The x_1 and y_1 columns represent the bottom left corner of the integration region which extends to the point (x_2, y_2). The number of grid points in each of the directions of the x- and r- integration region directions is represented by the i and j columns. Two kinds of wavenumber regions can be specified as previously discussed. The first is when the wavenumber spectrum is required to be known at each radial location. The radial range of these values is specified in Table 3 by k_{y1} and k_{y2}. The column k_{x1} and k_{x2} are the streamwise locations where the wavenumber region starts and ends. If the values of k_{y1} and k_{y2} are specified then a line can be specified by the given point locations and the wavenumber integration region is based on the number of index values specified in k_{max}. The index wavenumber integration ranges are specified from k_1 to k_2. These values are chosen for the wavenumber integration to only encompass the spectral peaks that contribute to BBSAN. The wavenumber integration range is $k_1 dk < k < k_2 dk$.

The dualstream nozzle operating at $M_{jp} = 0.71$, $TTR_p = 2.14$, $M_{js} = 1.36$, and $TTR_s = 1.00$ is shown in Fig. 2. Part a) shows the computational domain for the RANS solution. Over-laid on the CFD computational domain are red boxes that represent the three integration regions described in Table 3. The first integration region is the longest one encompassing the fan shear layer, the second is near the fan nozzle outlet, and the third encompasses the primary jet core region. Integration grids constructed based on the index values are overlaid over the RANS grid. Note that the integration region grids are slightly more dense and are uniform relative to the CFD domain. Figure 2 part b) shows the same region of the flow-field but with contour plots of the shock pressure, p_s. The shock pressure from the CFD solution is shown outside the integration regions and the interpolated p_s is shown inside the three integration regions. Integration regions cover all variation of p_s in the plume, however, on the outside of the core nozzle there is a small region that is not integrated. This isn't an issue due to the fact that turbulence in this region will not contribute to BBSAN. Figure 2 part c) shows the turbulent kinetic energy K over the same region. Contours of K outside the integration regions are from the RANS solution and inside the integration regions are interpolated values. Clearly, the vast majority of the turbulence in this case exists in the shear layer between the ambient and the fan stream. p_s is also large in this region, and indeed, the vast majority of BBSAN is generated in the fan shear layer. By only integrating over certain BBSAN sources such as the fan-ambient shear layer or the jet-fan shear layer one can easily find the largest sources of BBSAN or the dominant ones. Finally, by selectively integrating over various parts of the wavenumber spectra as in Morris and Miller,[13] then one can find the different spectral contributions to each observer position from any region of the wavenumber spectrum.

The first dualstream BBSAN calculation is performed for a supersonic core stream with a high speed subsonic fan stream. This case is presented first because it is similar to a single stream jet with no free-stream velocity or to a jet noise test in an anechoic chamber with an ambient flight velocity. The jet is operating at $M_{jp} = 1.19$, $TTR_p = 1.80$, $M_{js} = 0.96$, and $TTR_s = 1.00$, and is shown in the first line of Table 1 and Table 3. Figure 3 shows the BBSAN prediction where the x-axis represents the Strouhal number, $St = fD_j/u_j$ and the y-axis represents the Sound Pressure Level (SPL) per unit St. Measurement and prediction are at a distance of $R/D_p = 100$ from the primary nozzle exit center. For each prediction the observer angle, θ, is shown and is measured from the downstream jet axis. Maximum SPL is also shown and is found by the maximum broadband value and not a screech tone. Experimental data from the

American Institute of Aeronautics and Astronautics

Boeing Company are shown as green lines while the BBSAN predictions are shown as thicker black lines. At $\theta = 90.0$, it is observed that the maximum BBSAN peak agrees extremely well with experiment near $St = 0.8$. At lower frequencies the predicted BBSAN falls off quickly. This region of the spectrum is dominated by mixing noise. The fall-off between experiment and prediction at this angle agrees extremely well up until $St = 6.0$. As the observer angle decreases towards the downstream axis the maximum magnitude of the BBSAN almost perfectly matches the experiment and starts to be dominated by mixing noise. For observers in the upstream direction the predicted magnitude and fall-off of BBSAN remains in fair agreement with experiment. Unfortunately, the predicted frequency and BBSAN width at the highest observer $\theta = 130$ does not agree with experiment. This is due to the effects of the addition of a high speed subsonic jet around the supersonic core jet. This signifies that refraction effects are modifying the radiated BBSAN noise, as the sources of BBSAN noise in this problem are essentially in the jet-fan shear layer. Note that refraction effects are almost negligible near the sideline direction and therefore the slideline predictions are more accurate.

For the second BBSAN calculation the same nozzle and jet conditions are used except for the fully expanded Mach number of the fan flow. This fan nozzle fully expanded Mach number is increased from $M_{js} = 0.96$ to $M_{js} = 1.09$. This results in a flow where the BBSAN sources are dominant in the jet-fan shear layer and are negligible in comparison to the fan-ambient shear layer. Figure 4 shows BBSAN predictions of $M_{jp} = 1.19$, $TTR_p = 1.80$, $M_{js} = 0.96$, and $TTR_s = 1.00$ for the same angles as the previous prediction. Just as in the previous case the prediction at $\theta = 90$ degrees is very good and matches the peak frequency, magnitude, and has the correct fall-off in the lower St region because of mixing noise dominance and good fall-off at higher St. As the observer angle decreases the mixing noise starts to dominant the spectrum and the main BBSAN peak decreases in magnitude and increases in St. As θ increases to the upstream jet direction the BBSAN peak becomes too narrow again and predicts lower peak frequencies than the experiment. The peak frequency mismatch at $\theta = 130$ is larger than the previous case. The dominant BBSAN sources in this flow and the previous one are relatively the same, however, the higher speed fan flow has caused additional refraction effects compared to the previous case. This results in an undesired frequency shift in the results while the magnitude of the BBSAN is predicted relatively correctly across all observer angles.

The opposite situation is now examined in which the fan stream is supersonic while the core stream is subsonic. The dualstream nozzle operates at $M_{jp} = 0.71$, $TTR_p = 2.14$, $M_{js} = 1.36$, and $TTR_s = 1.00$ that correspond to the conditions in Tables 1 and 3. At the sideline angle of $\theta = 90$ the BBSAN peak frequency has good agreement and the magnitude has excellent agreement. Fall-off at lower frequencies occurs as mixing noise dominates while at higher frequencies the fall-off is initially too steep. This could easily be fixed by increasing k_1. However, no attempt has been made to "tweak" or optimize the integration region or wavenumber region specifications. The results demonstrate the robustness of the prediction technique but require the initial careful selection of integration ranges. The high frequency over-prediction at high angles such as at $\theta = 130$ can be eliminated by increasing k_1 a few integers. The peak magnitudes and peak frequencies at most θ match extremely well, especially in the upstream direction. This is unlike the previous two BBSAN prediction cases because the dominant BBSAN sources exist in the fan-ambient shear layer and not the core-fan shear layer as pointed out by observing the regions of high K and p_s in Fig. 2. These fan-ambient shear layer BBSAN source locations do not propagate through a high speed shear layer. This is in contrast to the previous two cases. Therefore, the free-field Helmholtz Green's functions are an excellent approximation to use in the formulation of the model for this type of flow.

The next prediction, that is shown in Fig. 6, is made for the dualstream nozzle operating at $M_{jp} = 1.281$, $TTR_p = 2.87$, $M_{js} = 0.848$, and $TTR_s = 1.00$. Here the core jet is heated and supersonic while the fan stream is subsonic and cool. The prediction agrees extremely well with the Boeing measurements at all observer angles and magnitudes. Unfortunately, the high speed fan flow has shifted the prediction at $\theta = 130$ degrees a small amount to a lower St. However, the slightly low frequency predictions at very high observer angles could easily be corrected by a simple empirical formula.

Predictions are shown for a final case where both streams are supersonic. This jet is shown in Fig. 7 with operating conditions $M_{jp} = 1.281$, $TTR_p = 2.87$, $M_{js} = 1.20$, and $TTR_s = 1.00$. In the experimental data it is now clear that there are two BBSAN peaks. One from the jet-fan shear layer sources and the second from the fan-ambient shear layer sources. These are very apparent in the upstream direction, for example at $\theta = 120$ degrees at $St = 0.18$ and $St = 0.35$. At $\theta = 90$ the predicted peak magnitudes align well with the experiment. In this case the contribution to the total prediction from the BBSAN sources in the jet-fan shear layer are plotted as orange lines while the contribution to the total prediction from BBSAN sources

American Institute of Aeronautics and Astronautics

in the fan-ambient shear layer are plotted in blue. Near $\theta = 90$ both of these individual peaks align well in frequency and magnitude with experiment. Since the off-design parameter for the primary jet is greater than the secondary, the magnitude of the jet-fan shear layer sources produces greater BBSAN as can be observed at all the angles. Also, since the fan jet stream off-design parameter is lower, the shock cell spacing is smaller and produces the lower St peaks. As the observer angle is increased towards the downstream direction the mixing noise dominates and the BBSAN forms less of a contribution to the total noise. In the upstream direction the total BBSAN prediction is again frequency shifted to lower frequencies than the experiment as seen in previous predictions. However, the peak frequencies of the fan-shear layer sources match exactly with the BBSAN peaks in the experimental data. This is unlike the lower predicted BBSAN peaks relative to the experimental data for the jet-fan BBSAN sources. It is due to the fact that the mean flow effects are negligible for the fan-ambient shear layer sources while the jet-fan shear layer sources need to propagate through the supersonic shock containing jet-fan stream.

The final dualstream nozzle prediction is shown in Fig. 8 and is operating at $M_{jp} = 1.281$, $TTR_p = 2.87$, $M_{js} = 1.36$, and $TTR_s = 1.00$. Relative to the previous case, the fan stream off-design parameter is slightly larger than the jet stream off-design parameter. At the sideline direction the two peaks in the experimental data from both the axial and co-axial jets can be observed at approximately $St = 0.25$ and $St = 0.42$. The total BBSAN prediction identifies these peaks with regards to magnitude and St. The fall-off is excellent at higher St. In the upstream direction the magnitude and St of the fan-ambient shear layer source BBSAN peak is well represented, though the second BBSAN peak is not.

Rectangular Nozzle BBSAN Calculations

Thus far axisymmetric single and dual stream CFD RANS solutions have been used to perform BBSAN predictions. These used the axisymmetric form of the BBSAN model equation and its implementation. Rectangular jet RANS-CFD solutions are obtained in the same fashion as the dualstream case, except that three dimensional calculations are performed. The flow predictions for both cold rectangular jets with $M_d = 1.50$ were validated with Pitot and schlieren comparisons. The experimental results and procedure are documented in Goss et $al.$[19] or Veltin.[20] The summary of the rectangular jet operating conditions are shown in Table 2. Since the aspect ratio of the nozzle is, $AR = 1.75$, some azimuthal dependence of the BBSAN is apparent in the experimental results. Here, predictions are only presented in the major axis plane, though results have also been found in the minor axis plane direction. Microphone positions were placed at 1.905 m from the jet at various observer angles in the minor and major axis planes and at an azimuthal angle, ϕ, of 45 degrees. The experimental data is extended to 100 D_e to be consistent with the predictions presented in the previous section for $R/D_e = 100$. The characteristic frequencies of the rectangular jets are based on the fully expanded equivalent diameter found from D_e and the NPR.

For the first BBSAN prediction the rectangular nozzle operates at $M_j = 1.30$ and $TTR = 1.00$ producing an over-expanded flow. The predictions are shown in Fig. 9. The integration and wavenumber parameters are shown in the first row of Table 4. The definitions of the columns are the same as Table 3 except for the addition of points and index values in the third direction. z_1 and z_2 are the starting and ending points of the integration region with k grid points. It is clear that screech tones are present in this jet and the turbulent velocity cross-correlations are different than those of a non-screeching jet. The calibration coefficients have been constructed with a heated non-screeching jet. This causes the small frequency mismatch at the sideline observer angle $\theta = 90$ but the peak frequency agreement is very good at high observer angles $\theta = 120$ and $\theta = 130$ degrees. All observer positions have excellent high and low frequency fall-off. At $\theta = 130$ and $St = 2$ there is a a slightly high "bump" in the prediction. This could easily be corrected by lowering slightly the wavenumber integration range value of k_1. Throughout the different observer angles the peak magnitude of the BBSAN show very good agreement with the experimental results but this comes at a cost of modifying P_f for all over-expanded jet calculations as mentioned before.

A second rectangular BBSAN prediction is made with the same nozzle but changes the fully expanded Mach number to $M_j = 1.70$ and retains $TTR = 1.00$. These under-expanded results are shown in Fig 10 and the integration and wavenumber region parameters are shown in the second row of Table 4. Once again the magnitudes and frequencies of the prediction match and scale with varying observer angle. Note that the jet is non-screeching. The experimental data of this case in particular show the primary BBSAN peaks with dominant higher frequency BBSAN peaks. The prediction accurately predicts these higher frequency peaks and scales them accordingly.

Figure 11 shows the prediction for the rectangular nozzle operating at $M_j = 1.70$ and $TTR = 2.20$

with integration and wavenumber parameters shown in the third row of Table 4. The same good agreement remains between the magnitude and frequency of the peak BBSAN. Higher frequency peaks of BBSAN can also be seen. The fall-off of predicted BBSAN is larger than the cold case at high St.

IV.   Conclusion

These BBSAN predictions of dualstream jets represent the first of their kind. There have been past successful predictions of the peak BBSAN frequencies or magnitude scaling of dualstream jets but not of the entire spectrum, its magnitude, its peak frequencies, and higher peak frequencies. Also, the method directly ties in the features of the flow-field and the nozzle geometry to the noise. The various BBSAN peaks and their magnitudes from both the jet-fan and fan-ambient shear layers have been identified. Several different combinations of off-design supersonic dualstream jets have been considered. These include the supersonic primary stream with subsonic fan stream, subsonic primary stream with supersonic fan stream, and both streams operating supersonically. When the core operates supersonically and the fan stream operates subsonically then the prediction is exactly like a single stream prediction but with a very high speed forward flight velocity. Some frequency mismatch occurs at observer angles in the forward quadrant and is not apparent in the downstream observer direction. This could easily be corrected with an empirical correction factor or calculating the Green's functions numerically. This second approach is already underway and is expected to improve the prediction quality of BBSAN when sources are located in the jet-fan shear layer.

This study also represents the first successful RANS based prediction of rectangular jets operating at two TTR in the over- and under-expanded regime. There is no restriction on the three dimensional nozzle geometry or operating conditions. Only one cross-stream length scale is built into the model. If the aspect ratio of the nozzle is large then it may be necessary to incorporate a second orthogonal cross-stream length scale to take into account the varying SPL as a function of azimuthal angle to the jet centerline axis.

The coefficients have been determined based on heated non-screeching jets. This approach is superior to calibrating the coefficients against screeching jets. Screech effects the BBSAN magnitude and frequency due to increasing the turbulence in the shear layer and changes the two point cross-correlation of the turbulent velocities. Coefficients of the length scales remain exactly the same between over- and under-expanded jets, however, the predictions improve when the time scale is slightly reduced. This has the effect of widening the BBSAN peaks in the over-expanded predictions. This is a necessary modification because the shock wave that is attached to the nozzle exit acts as a source of effective broadband noise and not BBSAN.

Changing the wavenumber spectra calculation for the shock pressure to a single line has greatly improved the speed of the prediction and also removed the necessity of interpolating the integration region. The calculations could easily be performed with no interpolation at all. This is because it is not necessary to know the wavenumber spectra at each radial location, but only in the region of the shear layer along the BBSAN sources. Finally, by taking the shock pressure as a line through the termination of each oblique shock wave in the shear layer, the BBSAN predictions have improved.

Acknowledgments

References

[1]Harper-Bourne, M. and Fisher, M. J., "The noise from Shock-Waves in Supersonic Jets," AGARD, 1973.

[2]SAE International, *SAE ARP876, Revision D. Gas Turbine Jet Exhaust Noise Prediction*, SAE International, Warrendale, PA, 1994.

[3]Zorumski, W. E., "Aircraft noise prediction program. Theoretical manual. Parts 1 and 2," NASA TM 83199, 1982.

[4]Tam, C. K. W., "Stochastic model Theory of Broadband Shock-Associated Noise from Supersonic Jets," *Journal of Sound and Vibration*, 1987, pp. 265–302.

[5]Tam, C. K. W. and Tanna, H. K., "Shock-Associated Noise of Supersonic Jets from Convergent-Divergent Nozzles," *J. Sound Vib.*, Vol. 81, No. 3, 1982, pp. 337358.

[6]Pack, D. C., "A note on Prandtls Formula for the Wavelength of a Supersonic Gas Jet," *Quarterly Journal of Applied Mathematics and Mechanics*, 1950.

[7]Tam, C. K. W., Jackson, J. A., and Seiner, J. M., "A Multiple-Scales Model of the Shock-Cell Structure of Imperfectly Expanded Supersonic Jets," *Journal of Fluid Mechanics*, Vol. 153, 1985, pp. 123–149.

[8]Tam, C. K. W. and Chen, K. C., "A Statistical Model of Turbulence in Two-Dimensional Mixing Layers," *Journal of Fluid Mechanics*, Vol. 92, 1979, pp. 303–326.

[9]Tam, C. K. W., "Broadband Shock-Associated Noise of Moderately Imperfectly-Expanded Supersonic Jets," *Journal of Sound and Vibration*, Vol. 140, No. 1, 1990, pp. 55–71.

[10]Abdelhamid, Y. A. and Ganz, U. W., "Prediction of Shock-Cell Structure and Noise in Dual Flow Nozzles," AIAA Paper 2007-3721, 2007.

[11]Tam, C. K. W., Pastouchenko, N., and Viswanathan, K., "Broadband Shock-Cell Noise from Dual Stream Jets," AIAA Paper 2008-2833, 2008.

[12]Tam, C. K. W. and Reddy, N. N., "Prediction Method for Broadband Shock-Associated Noise from Supersonic Rectangular Jets," *Journal of Aircraft*, Vol. 33, 1996, pp. 298–303.

[13]Morris, P. J. and Miller, S. A. E., "The Prediction of Broadband Shock-Associated Noise Using RANS CFD," AIAA Paper 2009-3315, 2009.

[14]Miller, S. A. E. and Veltin, J., "Assessment of Computational Fluid Dynamics for Supersonic Shock Containing Jets," *AIAA Journal*, Vol. 47, No. 11, 2009, pp. 2738 – 2746.

[15]Tam, C. K. W. and Auriault, L., "Mean flow refraction effects on sound radiated from localized sources in a jet," *Journal of Fluid Mechanics*, Vol. 370, 1998, pp. 149–174.

[16]Zaman, K. B. M. Q., Bridges, J. E., and Brown, C. A., "Excess Broadband Noise Observed with Overexpanded Jets," *AIAA Journal*, Vol. 48, No. 1, 2010, pp. 202–214.

[17]Menter, F. R., "Two-Equation Eddy-Viscosity Turbulence Models for Engineering Applications," *AIAA Journal*, Vol. 32, No. 8, 1994, pp. 1598 – 1605.

[18]Nelson, C., "An Overview of the NPARC Alliance's Wind-US Flow Solver," AIAA Paper 2010-27, 2010.

[19]Goss, A., Veltin, J., Lee, J., and McLaughlin, D. K., "Acoustic Measurements of High-Speed Jets from Rectangular Nozzle with Thrust Vectoring," *AIAA Journal*, Vol. 47, No. 6, 2009, pp. 1482–1490.

[20]Veltin, J., "Flow Field and Acoustic Measurements of Rectangular Supersonic Jets," AIAA Paper 2009-19, 2009.

Table 1. Dualstream nozzle operating conditions.

Case	NPR_p	M_{jp}	NPR_s	M_{js}	TTR_p	TTR_s
Dual3	2.40	1.19	1.80	0.96	2.70	1.00
Dual1	2.40	1.19	2.10	1.09	2.70	1.00
Dual4	1.40	0.71	3.00	1.36	2.14	1.00
Dual5	2.70	1.28	1.60	0.62	2.87	1.00
Dual6	2.70	1.28	2.40	1.19	2.87	1.00
Dual7	2.70	1.28	3.00	1.36	2.87	1.00

Table 2. Rectangular nozzle operating conditions.

NPR	M_j	TTR
2.77	1.30	1.00
4.94	1.70	1.00
4.94	1.70	2.20

Table 3. Dualstream nozzle integration parameters. All spatial values are in units of meters.

Case	Int.#	x_1	y_1	x_2	y_2	i	j	k_{x1}	k_{y1}	k_{x2}	k_{y2}	k_{max}	k_1	k_2
Dual3	1	0.0250	0.0001	1.0000	0.1000	400	100	0.0001	-	1.200	-	512	28	100
Dual1	1	0.0860	0.0001	0.6000	0.1000	300	075	0.0060	-	1.400	-	512	08	100
Dual4	1	-0.0105	0.0348	0.6000	0.0817	300	075	-0.0974	0.0777	0.4840	0.0360	512	14	181
-	2	-0.0973	0.0513	-0.0105	0.0817	100	075	-0.0974	0.0777	0.4840	0.0360	512	14	181
-	3	0.0500	0.0001	0.6000	0.0348	300	075	0.0001	0.063	0.4840	0.063	512	04	181
Dual5	1	0.0250	0.0001	1.0000	0.100	400	100	0.0001	-	1.200	-	512	30	100
Dual6	1	-0.0105	0.0424	0.4650	0.0817	300	075	-0.0974	0.0880	0.7000	0.0085	512	09	200
-	2	-0.0570	0.0513	-0.0105	0.0817	025	025	-0.0974	0.0730	0.7000	0.0050	512	10	200
-	3	0.1070	0.0001	0.4650	0.0424	300	075	0.0150	0.070	0.7000	0.060	512	09	200
Dual7	1	-0.0239	0.0424	0.4650	0.0817	300	075	-0.0974	0.0920	0.7000	0.0085	512	09	100
-	2	0.06420	0.0140	0.4650	0.0424	300	075	0.0300	0.070	0.7000	0.060	512	09	100

American Institute of Aeronautics and Astronautics

Table 4. Rectangular nozzle integration parameters. All spatial values are in units of meters.

Case	Int.#	x_1	y_1	z_1	x_2	y_2	z_2	i	j	k	k_{x1}	k_{x2}	k_{max}	k_1	k_2
Rec1	1	0.0001	0.0001	0.0001	0.1473	0.011	0.021	300	75	75	0.0001	0.25	512	20	166
Rec2	1	0.0001	0.0001	0.0001	0.1473	0.011	0.021	300	75	75	0.0001	0.25	512	07	110
Rec4	1	0.0001	0.0001	0.0001	0.1473	0.011	0.021	300	75	75	0.0001	0.25	512	10	223

American Institute of Aeronautics and Astronautics
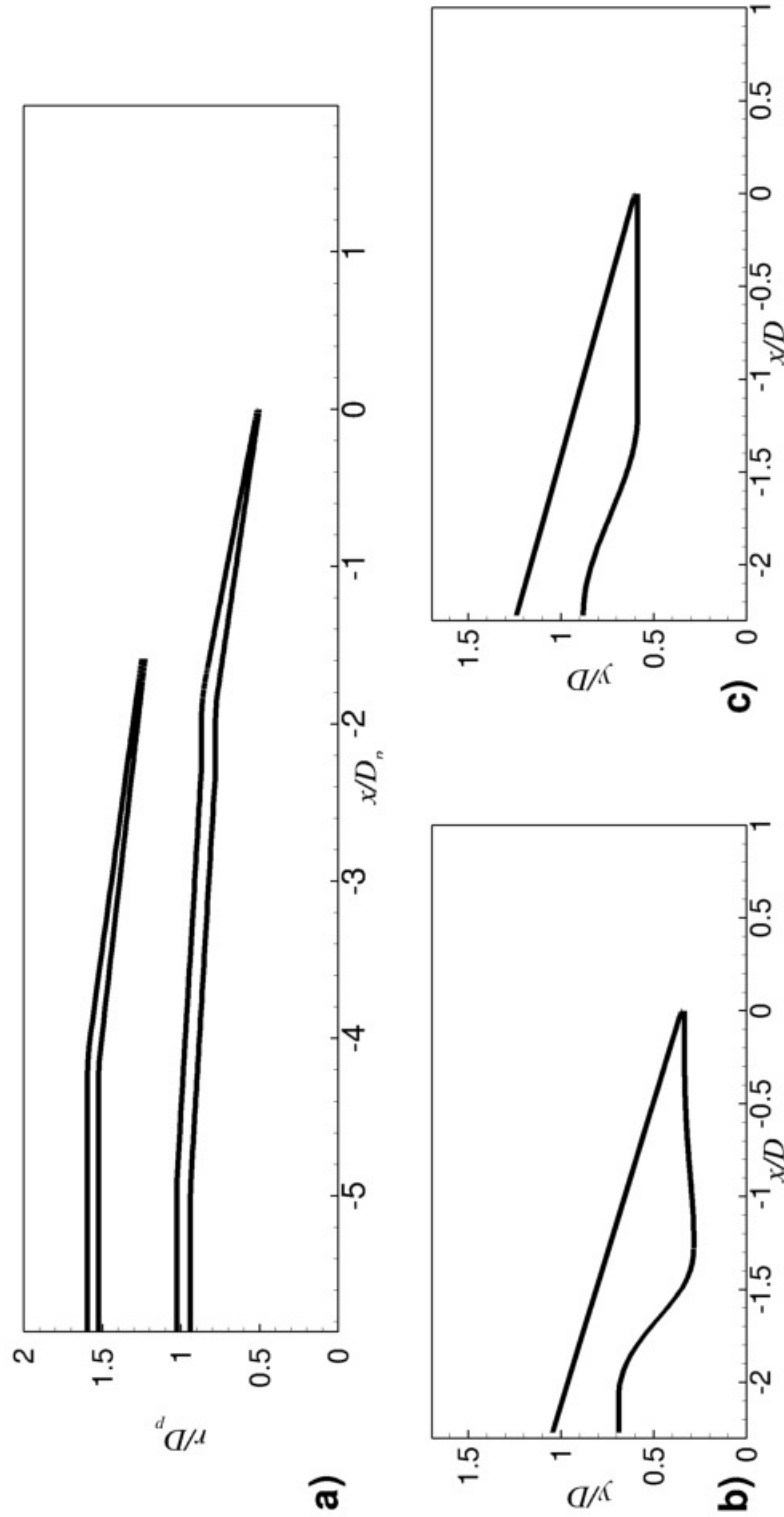
Figure 1. Contours of the nozzle surface about the nozzle centerline. a) Dualstream nozzle. b) Minor axis plane of the rectangular nozzle. c) Major axis plane of the rectangular nozzle.
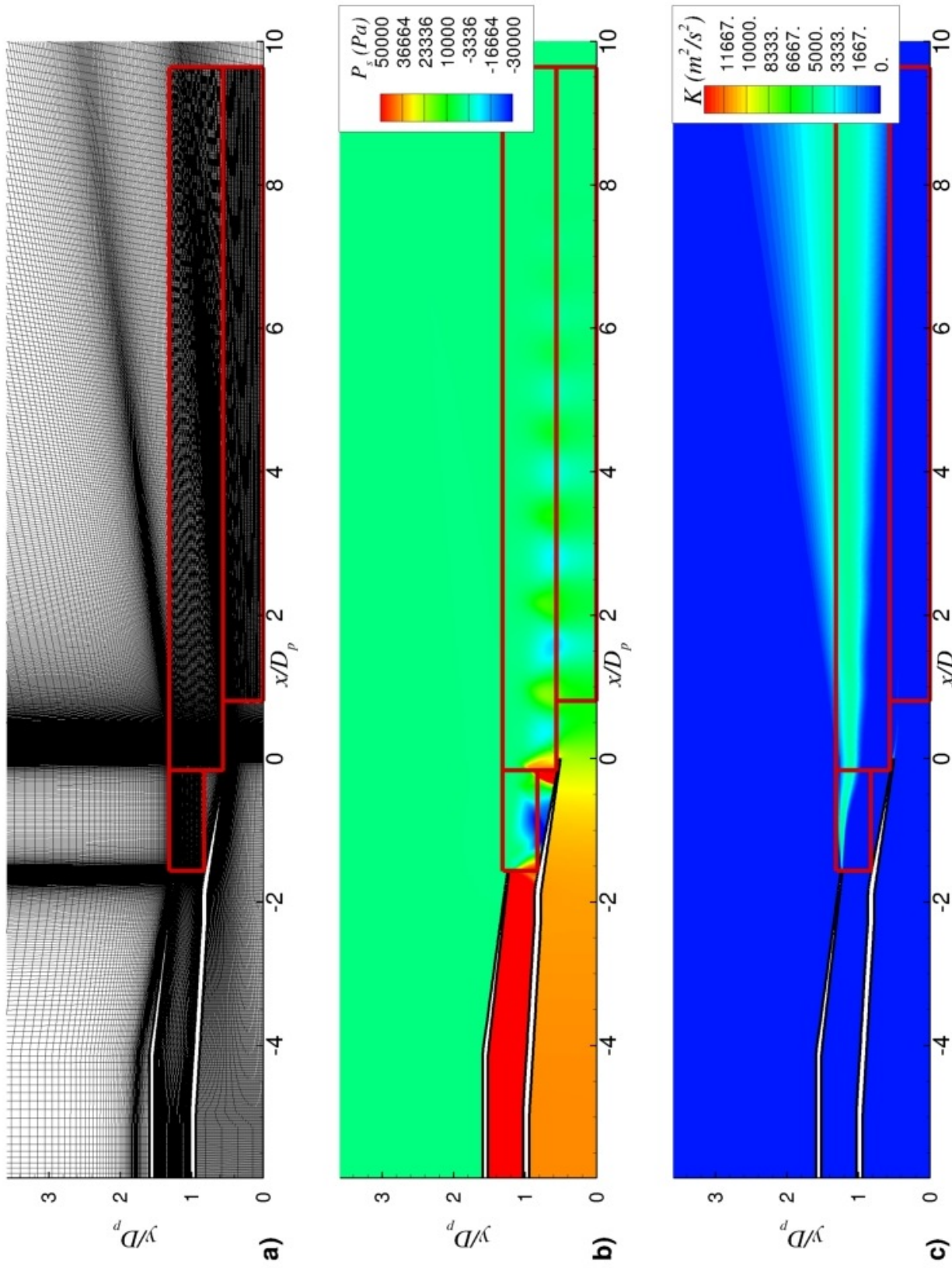
Figure 2. The dualstream nozzle operating at $M_{jp} = 0.71$, $TTR_p = 1.36$, $M_{js} = 2.14$, and $TTR_s = 1.00$. The red lines represent the three spatial integration regions necessary to calculate the BBSAN. Wavenumber integration regions are found by lines from near the nozzle lips and ending past the shock cell structure. Grids or contour plots inside each of the integration regions are superimposed on the RANS result. a) The computational domain for the RANS calculations and the three integration regions superimpose, b) the static pressure, c) the turbulent kinetic energy.

American Institute of Aeronautics and Astronautics
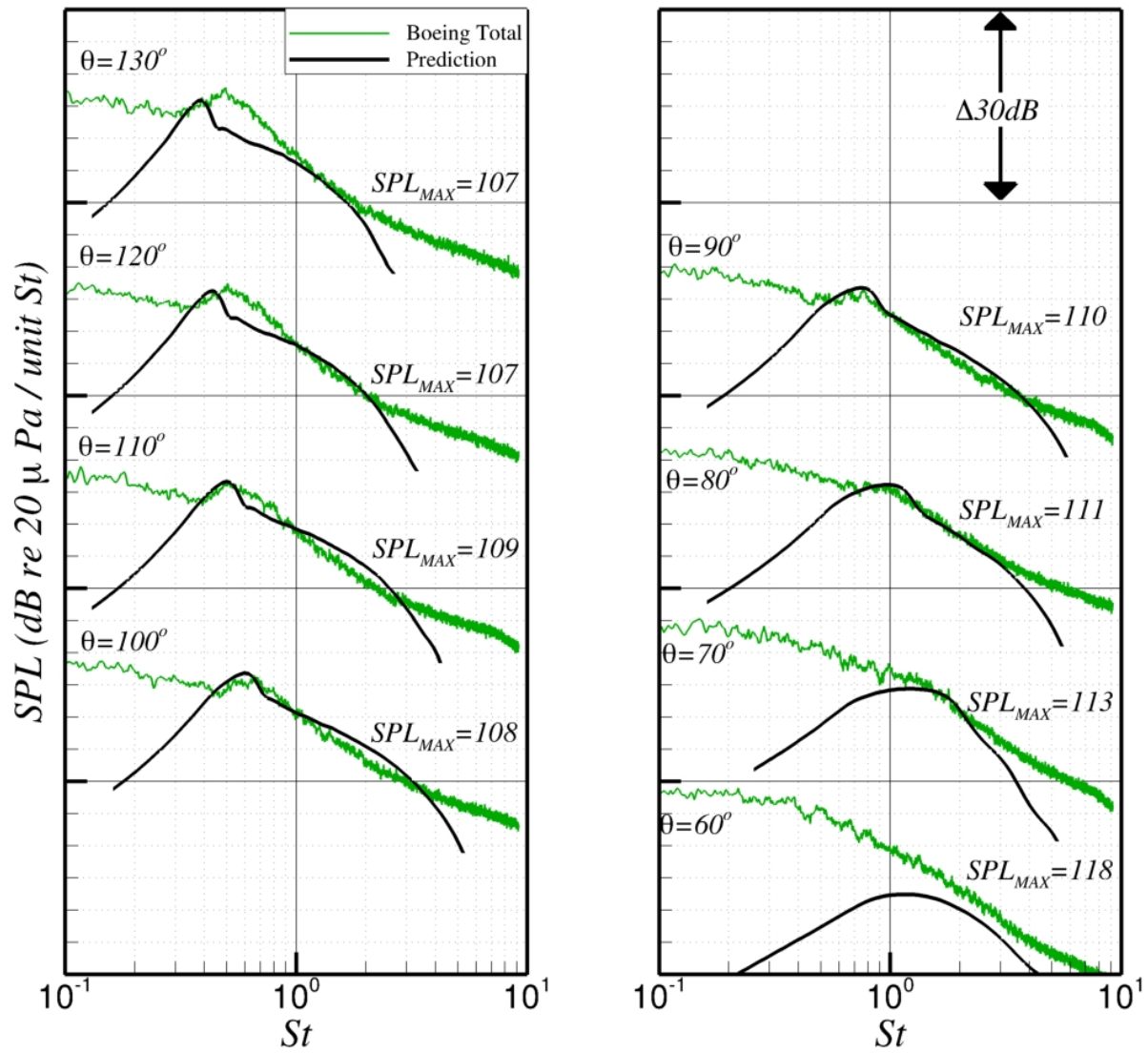
Figure 3. Predictions of the dualstream nozzle operating at $M_{jp} = 1.19$, $M_{js} = 0.96$, $TTR_p = 2.70$, and $TTR_s = 1.00$.
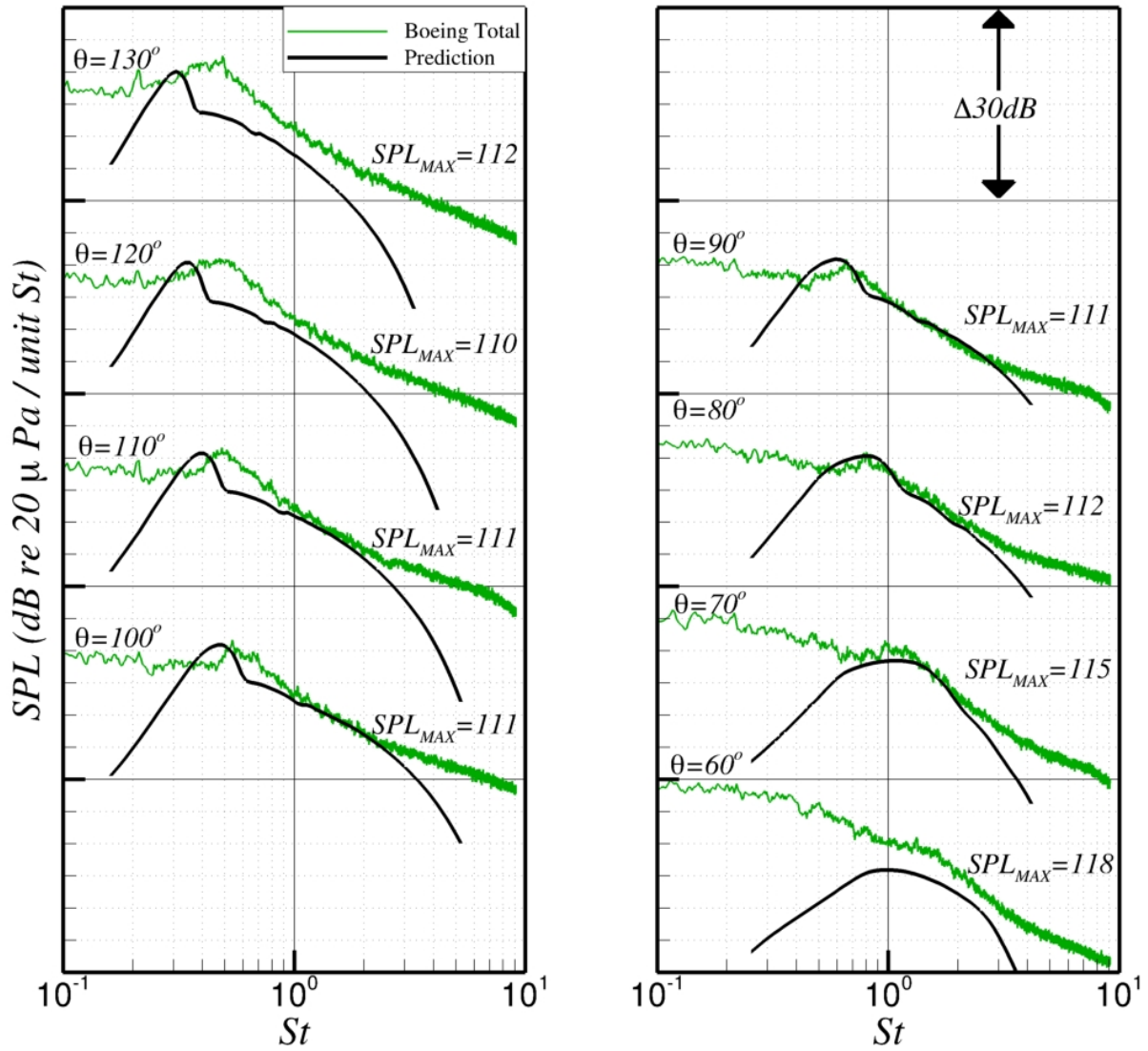
Figure 4. Predictions of the dualstream nozzle operating at $M_{jp} = 1.19$, $M_{js} = 1.09$, $TTR_p = 2.70$, and $TTR_s = 1.00$.
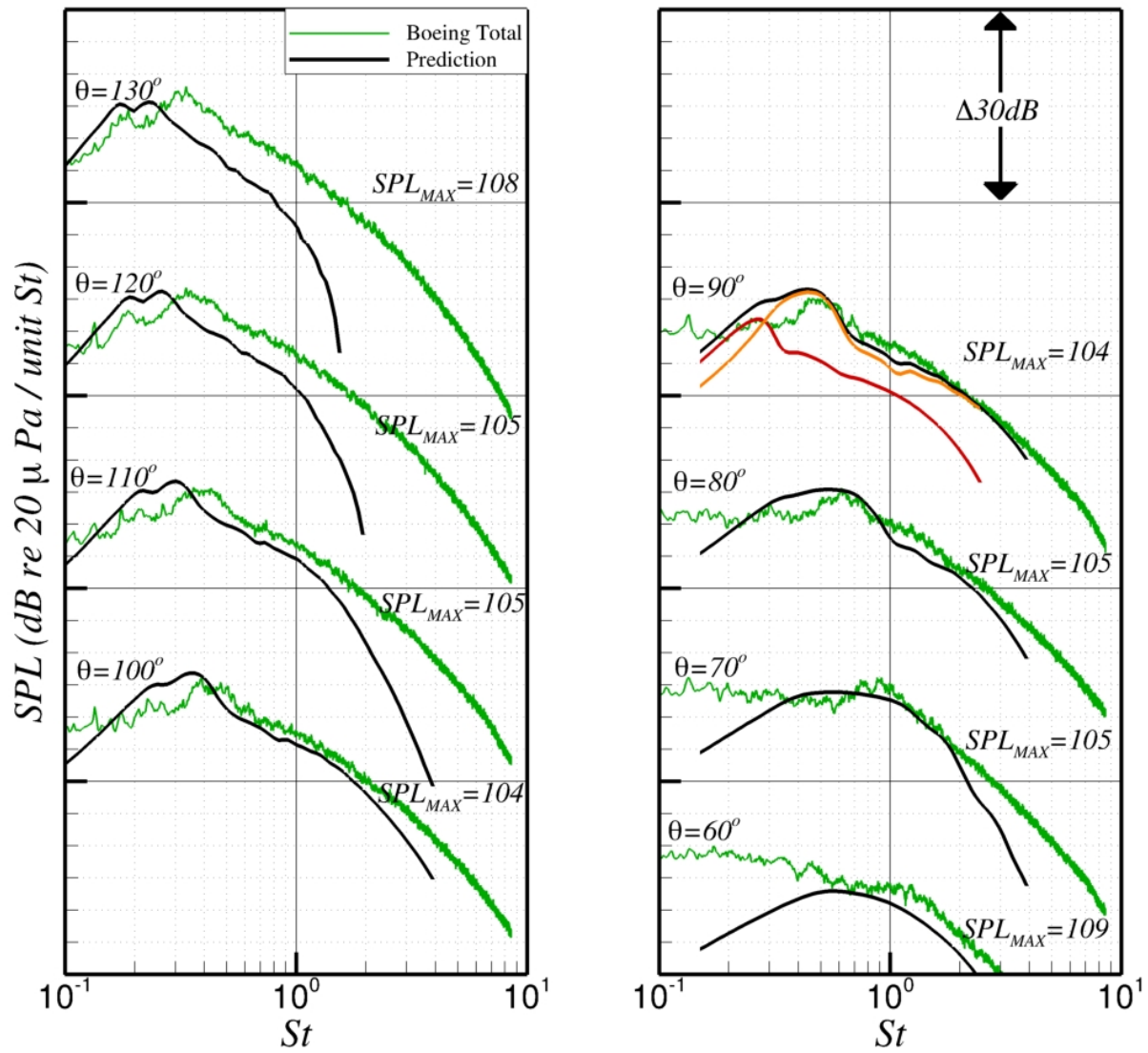
American Institute of Aeronautics and Astronautics
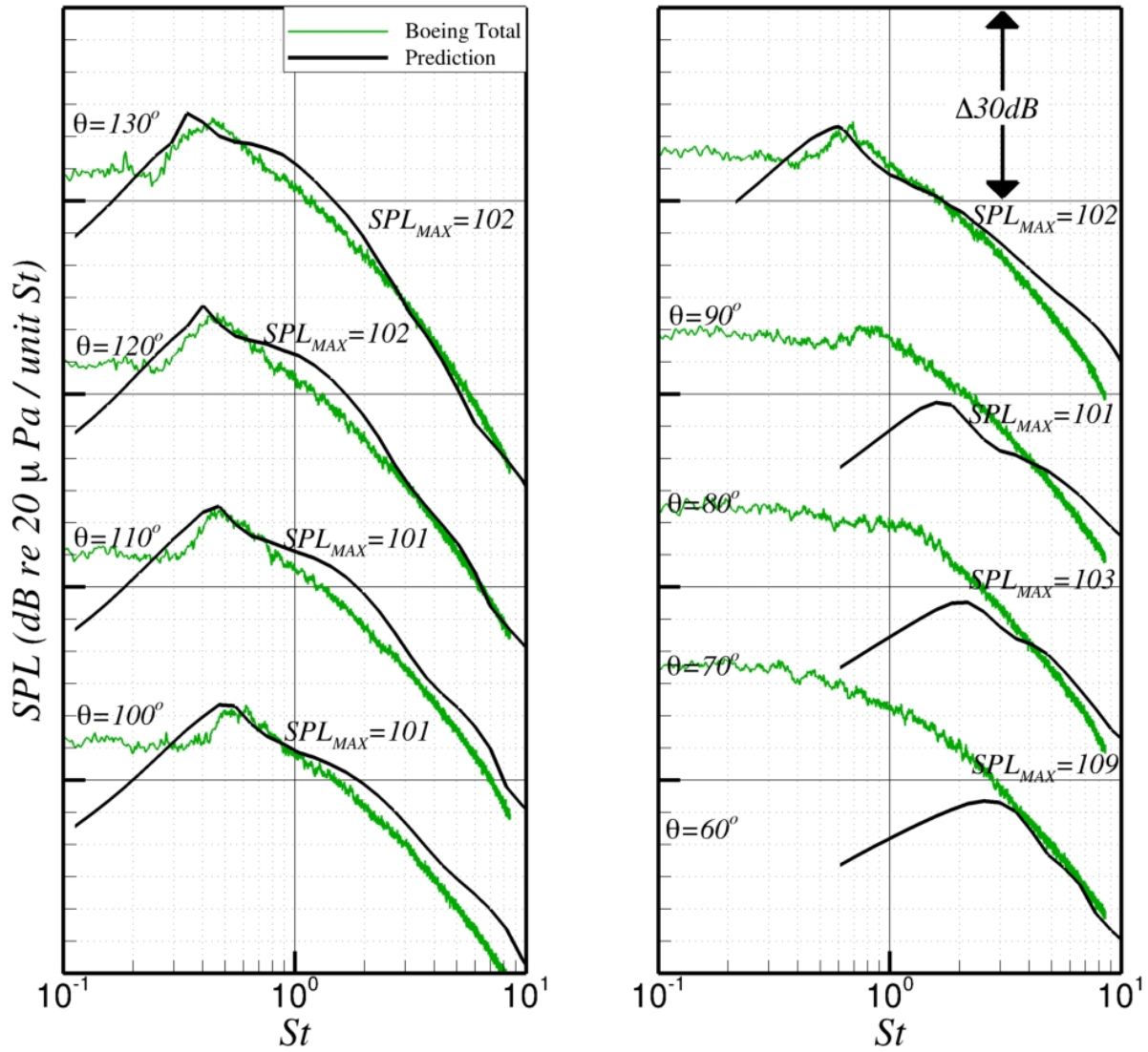
Figure 5. Predictions of the dualstream nozzle operating at $M_{jp} = 0.71$, $M_{js} = 1.36$, $TTR_p = 2.14$, **and** $TTR_s = 1.00$**.**

American Institute of Aeronautics and Astronautics
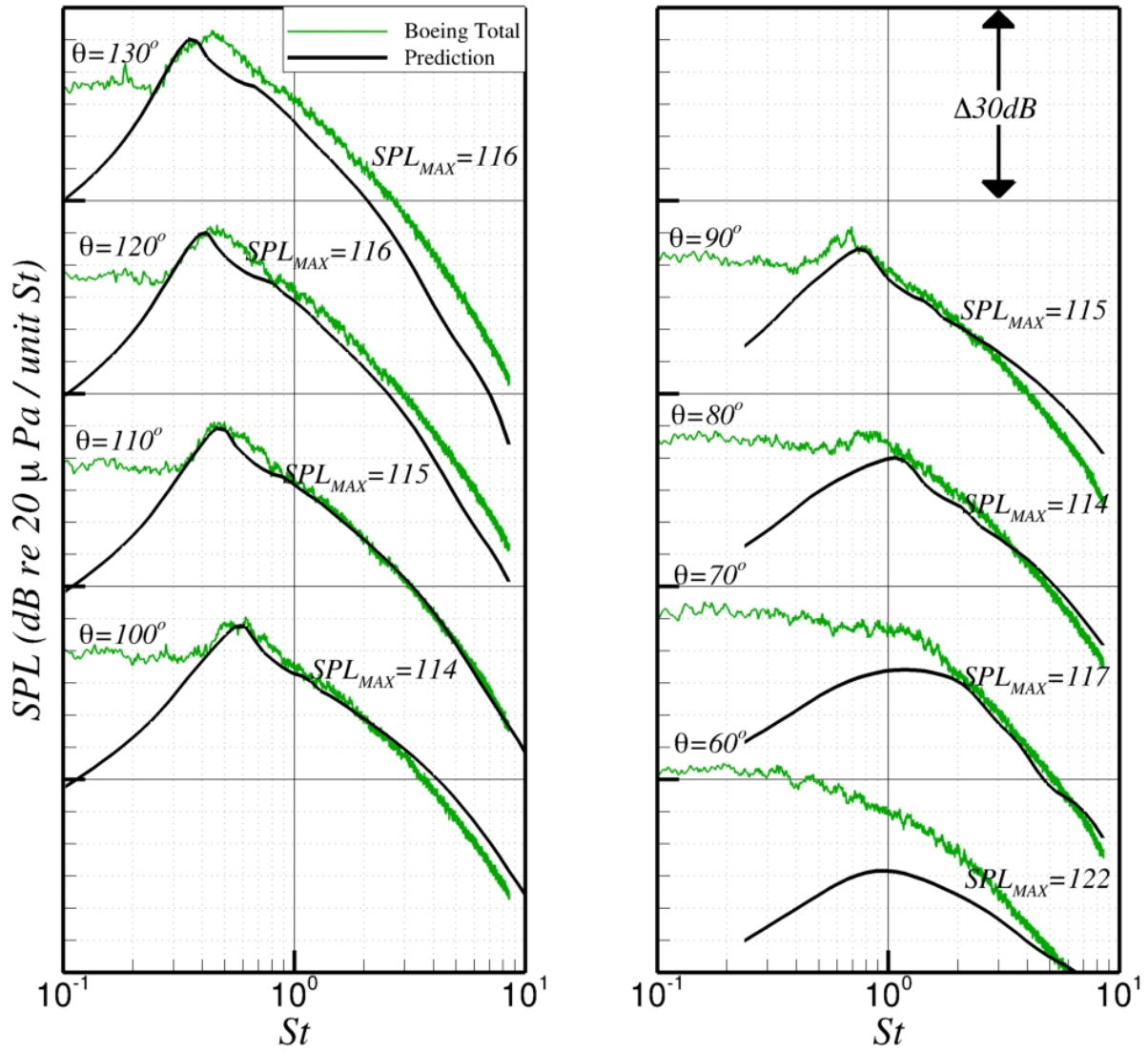
Figure 6. Predictions of the dualstream nozzle operating at $M_{jp} = 1.281$, $M_{js} = 0.848$, $TTR_p = 2.87$, and $TTR_s = 1.00$.

American Institute of Aeronautics and Astronautics

Figure 7. Predictions of the dualstream nozzle operating at $M_{jp} = 1.281$, $M_{js} = 1.20$, $TTR_p = 2.87$, and $TTR_s = 1.00$.
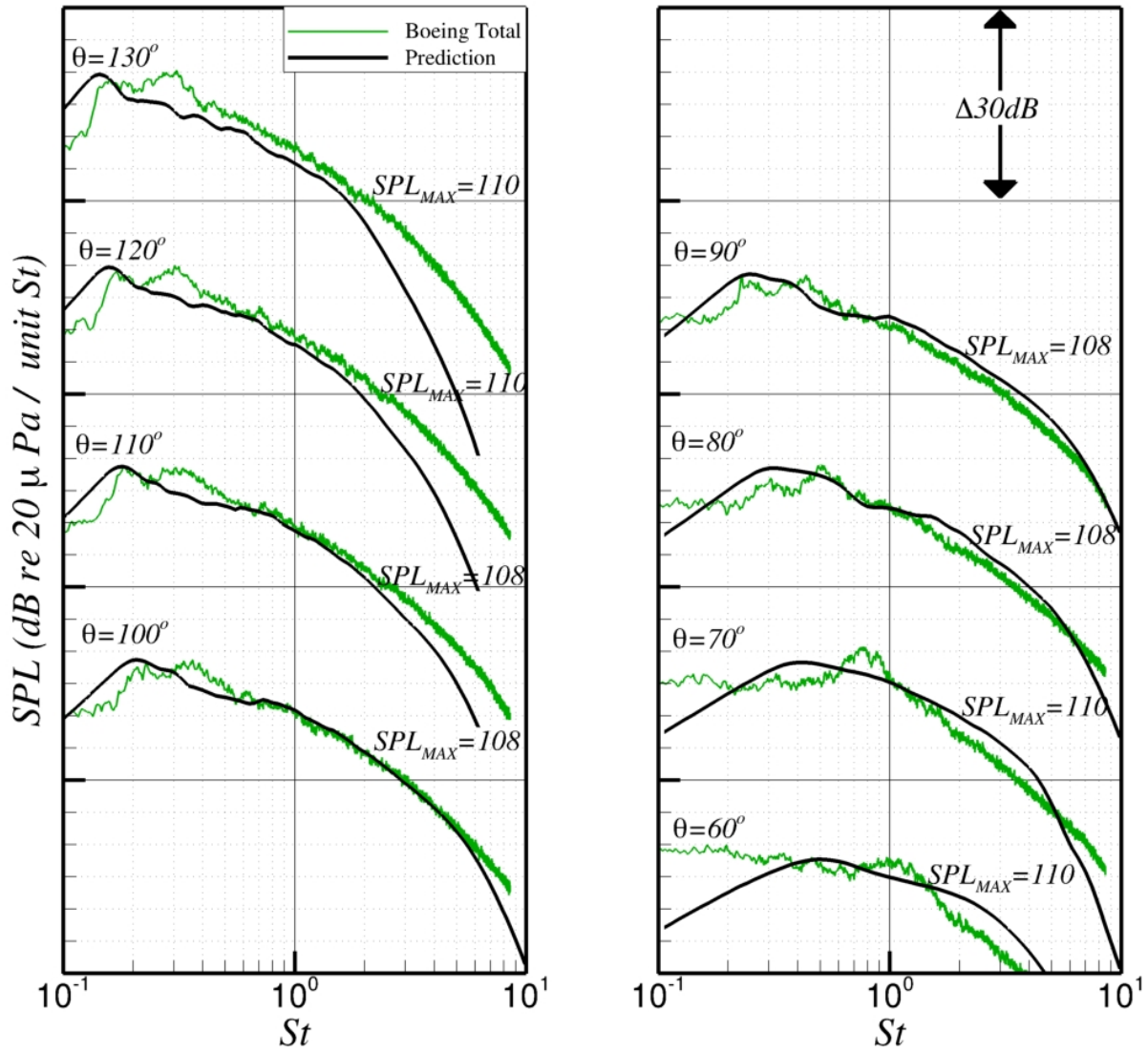
Figure 8. Predictions of the dualstream nozzle operating at $M_{jp} = 1.281$, $M_{js} = 1.36$, $TTR_p = 2.87$, and $TTR_s = 1.00$.
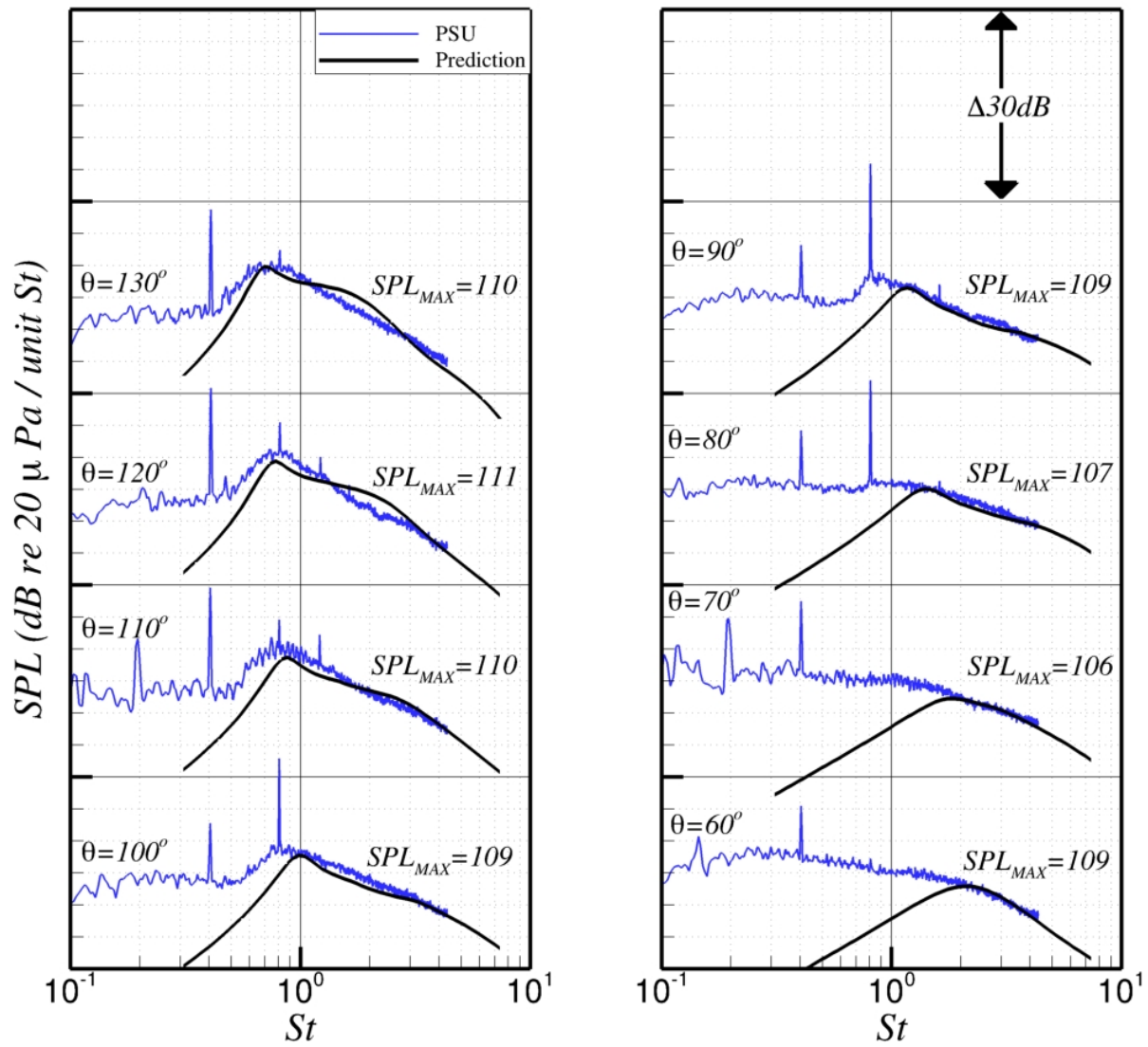
Figure 9. Predictions of the rectangular nozzle operating at $M_j = 1.30$, $TTR = 1.00$.
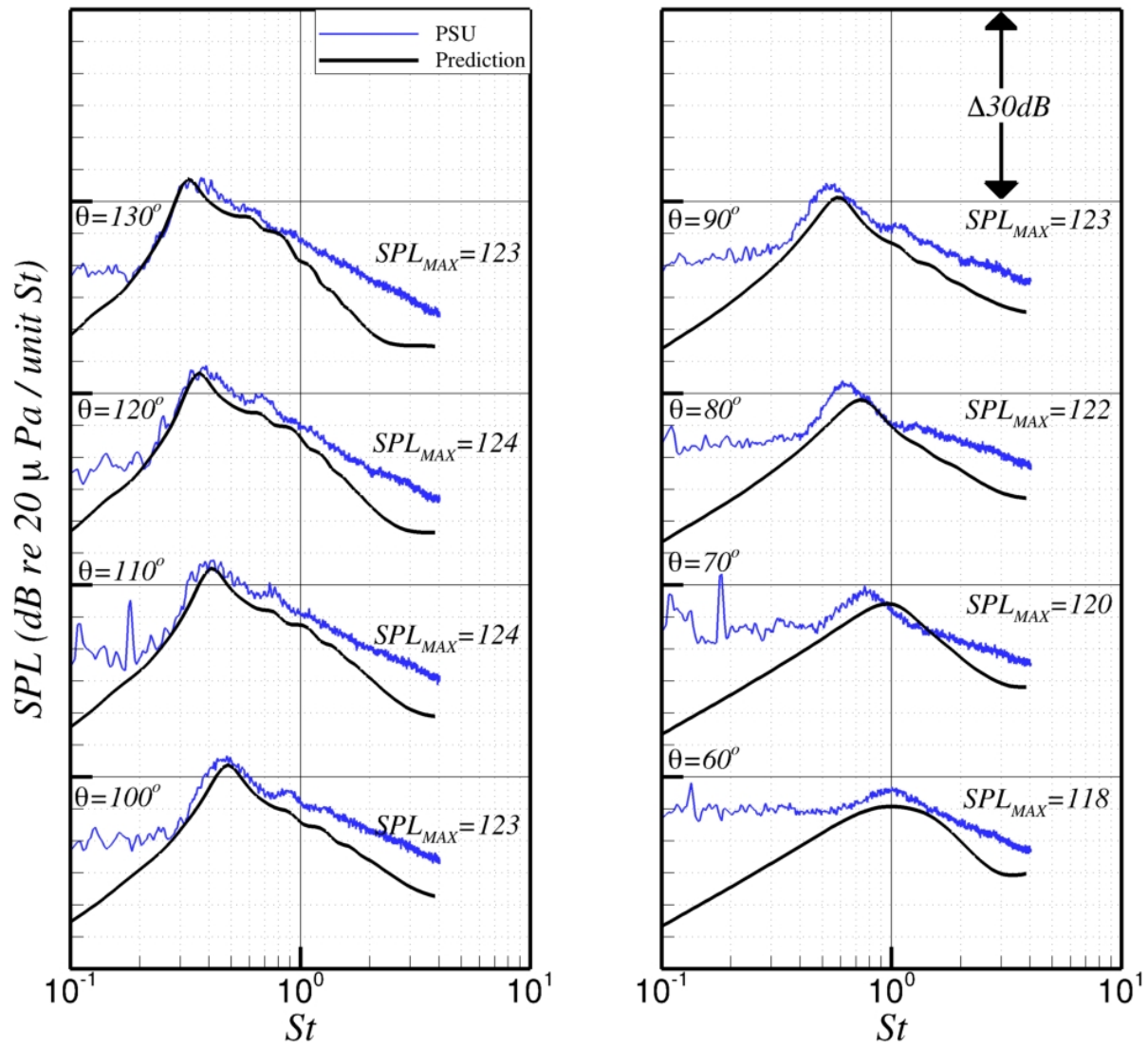
Figure 10. Predictions of the rectangular nozzle operating at $M_j = 1.70$, $TTR = 1.00$.
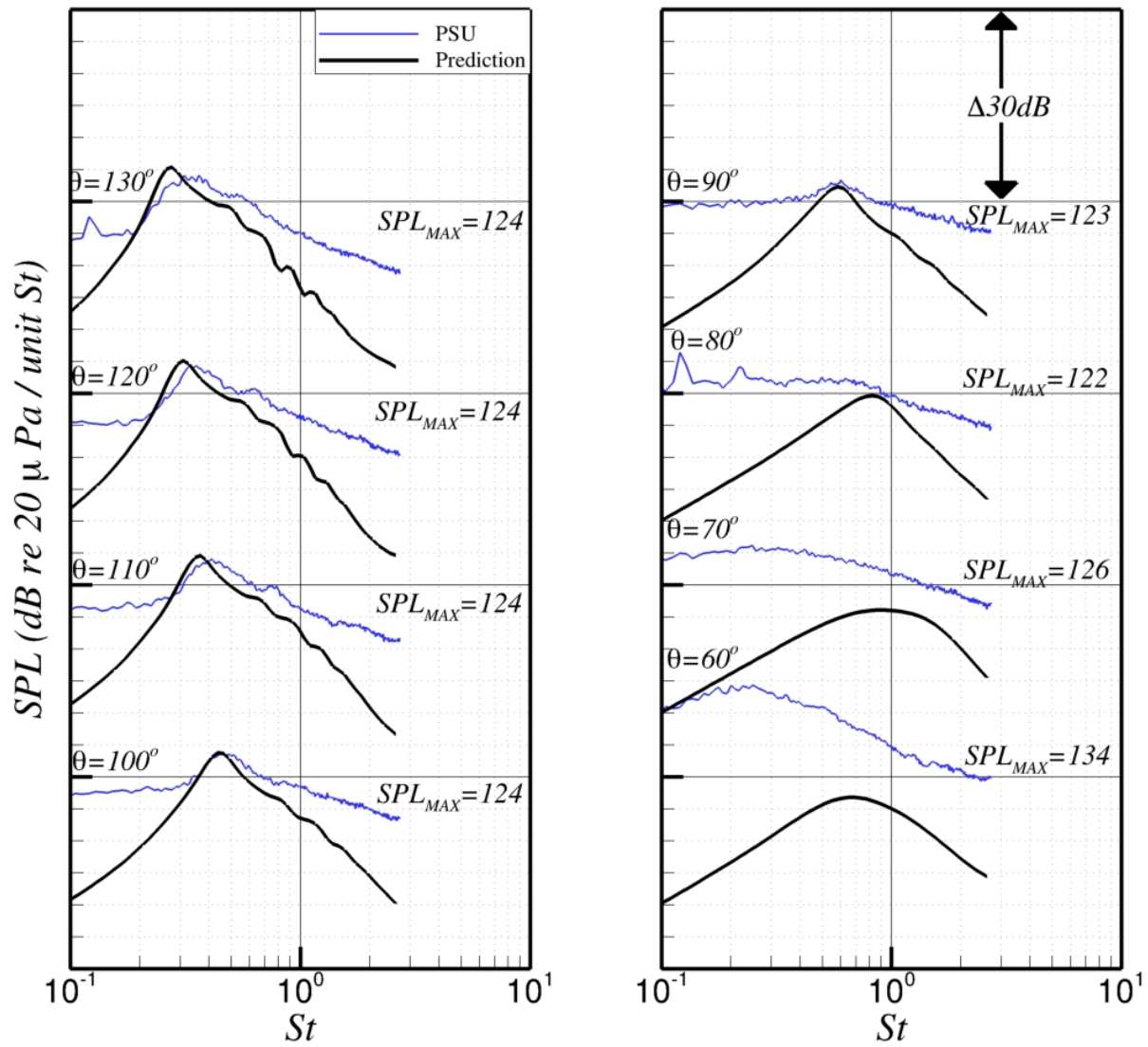
Figure 11. Predictions of the rectangular nozzle operating at $M_j = 1.70$, $TTR = 2.20$.

American Institute of Aeronautics and Astronautics